Journal of Inorganic Biochemistry 130 (2014) 38–51

Contents lists available at ScienceDirect

Journal of Inorganic Biochemistry

journal homepage: www.elsevier.com/locate/jinorgbio

A bismuth diethyldithiocarbamate compound promotes apoptosis in HepG2 carcinoma, cell cycle arrest and inhibits cell invasion through modulation of the NF-κB activation pathway

Dayang Hazwani Abang Ishak [a], Kah Kooi Ooi [b], Kok-Pian Ang [b], Abdah Md Akim [b,*], Yoke-Kqueen Cheah [b], Norshariza Nordin [c], Siti Nadiah Binti Abdul Halim [a], Hoi-Ling Seng [a], Edward R.T. Tiekink [a,**]

[a] Department of Chemistry, University of Malaya, 50603 Kuala Lumpur, Malaysia
[b] Department of Biomedical Science, Faculty of Medicine and Health Sciences, University Putra Malaysia, 43400 Serdang, Selangor, Malaysia
[c] Department of Obstetrics and Gynaecology, Faculty of Medicine and Health Sciences, University Putra Malaysia, 43400 Serdang, Selangor, Malaysia

ARTICLE INFO

Article history:
Received 16 July 2013
Received in revised form 26 September 2013
Accepted 30 September 2013
Available online 10 October 2013

Keywords:
Bismuth
Apoptosis
Metallopharmaceuticals
Cell cycle
NF-κB

ABSTRACT

The compound with R = CH_2CH_3 in $Bi(S_2CNR_2)_3$ (1) is highly cytotoxic against a range of human carcinoma, whereas that with R = CH_2CH_2OH (2) is considerably less so. Both 1 and 2 induce apoptosis in HepG2 cells with some evidence for necrosis induced by 2. Based on DNA fragmentation, caspase activities and human apoptosis PCR-array analysis, both the extrinsic and intrinsic pathways of apoptosis have been shown to occur. While both compounds activate mitochondrial and FAS apoptotic pathways, compound 1 was also found to induce another death receptor-dependent pathway by induction of CD40, CD40L and TNF-R1 (p55). Further, 1 highly expressed DAPK1, a tumour suppressor, with concomitant down-regulation of XIAP and NF-κB. Cell cycle arrest at the S and G_2/M phases correlates with the inhibition of the growth of HepG2 cells. The cell invasion rate of 2 is 10-fold higher than that of 1, a finding correlated with the down-regulation of survivin and XIAP expression by 1. Compounds 1 and 2 interact with DNA through different binding motifs with 1 interacting with AT- or TA-specific sites followed by inhibition of restriction enzyme digestion; 2 did not interfere with any of the studied restriction enzymes.

1. Introduction

Various bismuth compounds, e.g. bismuth subgallate and bismuth subnitrate, have been used in the past to treat hypertension, syphilis, gastrointestinal disorders and skin conditions [1–3]. In particular, since the 1970s, two bismuth compounds, i.e. bismuth subsalicylate (BSS, Pepto-Bismol®; the Procter & Gamble Company, Cincinnati, Ohio, USA), for the prevention and treatment of dyspepsia and diarrhoea, and colloidal bismuth subcitrate (CBS, De-Nol®; Gist Brocades, Delft, The Netherlands), for the treatment of peptic ulcers, have gained widespread use as OTC (over the counter) drugs emphasising the non-toxic nature of bismuth, at least in medicinal doses [4–6]. These bismuth-containing drugs as well as ranitidine bismuth citrate (Tritec® and Pylorid®) are being used worldwide in combination with antibiotics to eradicate infection due to *Helicobacter pylori* [4–6]. Complimenting clinical applications, new molecular bismuth compounds are under development as anti-cancer agents [7], of direct relevance to the present study, anti-viral agents [8], anti-microbials [9], for activity against the Leishmaniasis protozoa [10] and for the targeting of *H. pylori* [11].

Despite the widespread use of bismuth compounds in medicine and the efforts devoted to developing new bismuth compounds for the treatment of a variety of diseases, the biochemistry of bismuth is poorly understood [12,13]. Work has commenced to delineate the biocoordination chemistry of bismuth involving proteins, enzymes and cell membranes in order to redress the deficiency in knowledge concerning possible mechanisms of actions. It seems that the major target sites of bismuth in proteins and enzymes are both iron(III) sites in transferrin (having oxygen and nitrogen donors) [14,15] and zinc(II) sites in metallothionein (with thiolate donors) [16]. It is also well established that bismuth forms very stable complexes with glutathione, which may be involved in the transport of bismuth in cells and bacteria [17,18].

In connection with the anti-cancer potential of bismuth compounds, bismuth can be used as a protective agent in that pre-administration with bismuth is thought to protect patients from some of the toxic side-effects induced by the widely used anti-cancer drug, cisplatin, without affecting anti-tumour activity [19]. In terms of developing new drug candidates based on bismuth, interest is increasing with bismuth thiolates at the fore [20]. For example, studies on bismuth xanthate compounds of the general formula $Bi(S_2COR)_3$, for R = Et, i-Pr and cyclohexyl, were shown to exert cytotoxic activities against cisplatin-

* Corresponding author.
** Corresponding author. Tel.: +60 3 7967 6775; fax: +60 3 7967 4193.
E-mail addresses: abdah@medic.upm.edu.my (A.M. Akim), Edward.Tiekink@um.edu.my, Edward.Tiekink@gmail.com (E.R.T. Tiekink).

0162-0134/$ – see front matter © 2013 Elsevier Inc. All rights reserved.
http://dx.doi.org/10.1016/j.jinorgbio.2013.09.018

sensitive Calu-6 (human lung adenocarcinoma cells) and cisplatin-insensitive MCF-7 (human breast carcinoma cells) [21]. Subsequently, related species derived from the reaction of an amine with carbon disulphide with subsequent reaction with bismuth salts, i.e. bismuth dithiocarbamates with the general formula $Bi(S_2CNR_2)_3$, were also demonstrated to exhibit potent in vitro cytotoxicity against a panel of seven human cancer cell lines [22]. One species in particular, i.e. $Bi(S_2CNEt_2)_3$ (1, Fig. 1), proved to be very potent with activity comparable to that exhibited by taxol®. Therefore, this was chosen for in vivo anti-tumour screening against ovarian (OVCAR-3) and colon carcinoma (HT-29) cell lines in a murine model and proved to exhibit some anti-tumour activity [22]. Compound 1 and hydroxyl derivative, $Bi[S_2CN(CH_2CH_2OH)_2]_3$ (2, Fig. 1), form the focus of the present investigation.

Herein, in vitro cytotoxicity of 1 and 2 has been evaluated against a series of six human carcinoma cells, namely HepG2, MCF-7R, A2780, HT-29, A549 and 8505C. Having exhibited particular potency against HepG2, an investigation whether 1 inhibited the cell growth of HepG2 cells by regulating the cell cycle was conducted; non-potent 2 was also investigated in this regard. In addition, the underlying molecular mechanisms of the different growth-inhibitory effects of 1 and 2 in HepG2 cells were conducted in order to better understand their effects on the expression of several genes significantly involved in liver cancer development, and especially in the human cell cycle and apoptosis. The expression of these genes was quantified by polymerase chain reaction (PCR) microarray analysis. This study indicates the potential utility of bismuth compounds as a potent class of experimental therapeutics for liver cancer and lays the foundation for the rational design of new drugs based on bismuth.

2. Materials and methods

2.1. Instrumentation

^1H and $^{13}C\{^1H\}$ NMR spectra were recorded in a $CDCl_3$ solution at 25 °C on a Bruker Avance 400 spectrometer; abbreviations for NMR assignments: *t*, triplet, *q*, quartet and *m*, multiplet. IR spectra were obtained as KBr pellets on a Perkin Elmer RX1 FTIR spectrophotometer; abbreviations for IR assignments: *s*, strong, *m*, medium and *br*, broad. Elemental analyses were performed on a Perkin Elmer PE 2400 CHN Elemental Analyser. Melting points were determined on a Krüss KSP1N melting point apparatus. Powder X-ray diffraction (PXRD) data were recorded with a PANalytical Empyrean XRD system with Cu-Kα1 radiation (λ = 1.54056 Å) in the 2θ range 5 to 40° with a step size of 0.026°. Comparison between experimental and calculated (from CIF's) PXRD patterns was performed with X'Pert HighScore Plus [23].

2.2. Reagents and synthesis

The sodium salt of diethyldithiocarbamate, $Na[S_2CNEt_2]$ (10.00 mmol, 2.25 g; Sigma-Aldrich) was dissolved in distilled water (40 ml) and added slowly to a suspension of $BiCl_3$ (3.39 mmol, 1.069 g; R&M Chemicals) in ethanol (25 ml). After 2 h of stirring, a bright-yellow precipitate was obtained. This was then recrystallised from a $CH_3CN/CHCl_3$ (1:3) solution yielding a bright-yellow crystalline material, $Bi(S_2CNEt_2)_3$ (1), after the solution was left to stand overnight. Percentage yield: 93%. M.P. = 195 °C. Elemental analysis: Found C, 27.57; H, 4.72; N, 6.41. $C_{15}H_{30}BiN_3S_6$ requires: C, 27.56; H, 4.63; N, 6.43. IR (KBr disk, cm^{-1}): 1489 *m* ν(C–N); 1065 *s* and 906 *s* ν(C–S). ^1H NMR: δ 3.83 (*q*, CH_2, J = 7.2 Hz); 1.33 (*t*, CH_3, J = 7.1 Hz). $^{13}C\{^1H\}$ NMR: δ 202.0 (CS_2); 48.5 (CH_2); 12.0 (CH_3).

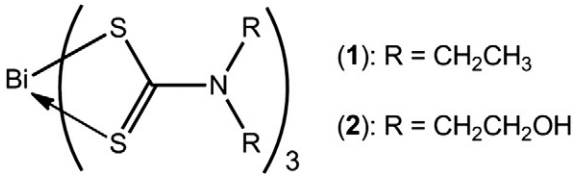

Fig. 1. The structures of $Bi(S_2CNEt_2)_3$ (1) and $Bi[S_2CN(CH_2CH_2OH)_2]_3$ (2).

The potassium salt of the di-hydroxylethyldithiocarbamate anion, $K[S_2CN(CH_2CH_2OH)_2]$, was synthesized by the reaction of diethanolamine (0.06 mol, 4.82 ml; Sigma-Aldrich), carbon disulfide (0.06 mol, 3.02 ml; Merck) and potassium hydroxide (0.06 mol; Riendemann Schmidt) in distilled water (40 ml). The salt (10.00 mmol, 2.19 g) was added to a suspension of $BiCl_3$ (3.39 mmol, 1.069 g) in ethanol (25 ml). After 2 h of stirring, the product was left overnight after which yellow-brown crystals of $Bi[S_2CN(CH_2CH_2OH)_2]_3$ (2) deposited. Percentage yield: 61%. M.P. = 157–158 °C. Elemental analysis: Found C, 23.79; H, 3.45; N, 5.51. $C_{15}H_{30}BiN_3O_3S_6$ requires: C, 24.03; H, 4.03; N, 5.61. IR (KBr disk, cm^{-1}): 3251 *br* ν(O–H); 1472 *s* ν(C–N); 1205 *s* ν(C–O); 967 *m* ν(C–S). ^1H NMR: δ 4.79 (*t*, OH, J = 5.4 Hz); 3.90 (*t*, NCH_2, J = 6.0 Hz); 3.73 (*m*, CH_2O). $^{13}C\{^1H\}$ NMR: δ 203.0 (CS_2); 59.0 (NCH_2); 57.0 (OCH_2).

2.3. Cell viability assay

The HepG2 (human hepatocellular carcinoma), MCF-7R (human breast carcinoma cells, multidrug resistant strain, Michigan Cancer Foundation-7), A2780 (human ovarian carcinoma), HT-29 (human colon adenocarcinoma), A549 (human lung adrnocarcinoma) and 8505C (human thyroid carcinoma) cell lines were obtained from ATCC: The Global Bioresource Center and maintained in culture as described by the provider. The cells were routinely grown in an RPMI 1640 medium containing 10% foetal calf serum (FCS) and anti-biotics at 37 °C and 6% CO_2. For evaluation of growth inhibition tests, the cells were seeded in 96-well plates (Techno Plastic Products, TPP, Plastik für die Zellkultur, Switzerland) and grown for 24 h in a complete medium. The stock solutions of 1 and 2 were prepared by dissolving the compounds in 1 mL of DMSO to reach a concentration of 10^{-2} M. They were then diluted in an RPMI medium and added to the wells (100 μL) to obtain a final concentration ranging between 0 and 80 μM. DMSO at comparable concentrations, i.e. <1%, did not show any effects on cell cytotoxicity. Stock solutions of the compounds were diluted directly in a culture medium to the required concentration and added to the cell culture. After 24 h of incubation at 37 °C, 20 μL of a solution of MTT (3-[4,5-dimethylthiazole-2-yl]-2,5-diphenyltetrazolium bromide) in PBS (phosphate buffer saline, 2 mg mL^{-1}) was added to each well, and the plates were then incubated for 2 h at 37 °C. The medium was then aspirated and DMSO (100 μL) added to dissolve the precipitate. The absorbance of each well was measured at 580 nm using a 96-well microplate reader and compared to the values of control cells incubated without a test compound. The IC_{50} values for the inhibition of cell growth were determined by fitting the plot of the percentage of surviving cells against the drug concentration using a sigmoidal function (Origin v7.5™).

2.4. Membrane permeability study by AO/PI staining

HepG2 cells at a concentration of 5×10^3 cells/well in 96 well plates were treated with the IC_{50} concentration of each compound and incubated for 24 h. Untreated cells were included as a negative control. Treated cells were harvested from the culture flask. 1× EDTA free-PBS was used to wash the cells twice before transferring to a microcentrifuge tube. The cells were centrifuged at 1000 g for 10 min. Subsequently, the cells were suspended in 100 μL 1× PBS. Then, a 5 mg/mL AO (acridine orange, Sigma) and PI (propidium iodide, Sigma) mixture was added to the cells in a 1:1 ratio for staining. This was followed by chilling on ice for 10 min. The mixture (20 μL) was aliquoted onto a slide and covered with a cover slip and viewed under an Olympus BX-51 fluorescence microscope. Images were captured by an attached Olympus CMAD-2 camera.

2.5. DNA fragmentation analysis

For the DNA fragmentation assay, 2×10^6 HepG2 cells were treated with 0.53 μM (1) and 55.9 μM (2) in an RPMI medium for 24 h at 37 °C and 5% CO_2. The cells were harvested and centrifuged at 300 ×*g*/15 min/10 °C and washed with PBS. The cells were then re-suspended at a concentration of 1×10^6 cells mL^{-1} in an extraction buffer (10 mM TriseHCl, 0.1 M EDTA, 5 g mL^{-1} SDS) and treated with 20 mg L^{-1} RNase A at 37 °C for 60 min, followed by incubation with proteinase K (100 mg L^{-1}) at 37 °C for 60 min. An equal volume of saline solution (NaCl 6 M) was added to the cells followed by centrifuging at 13,000 ×*g* for 10 min. The supernatant was collected and two volume equivalents of ethanol (−20 °C) were added. The samples were centrifuged at 13,000 ×*g* for 30 min at 4 °C. The supernatant was then discarded and the pellets dissolved in TE buffer (1×). The DNA concentration and quality were analyzed by electrophoresis and UV/vis on a BioPhotometer Spectrophotometer UV/VIS (Eppendorf, Germany). The samples were applied to a 1.5% agarose gel and subjected to electrophoresis for 2 h at 80 V with running buffer of TAE. The gel was stained, destained, and photographed under UV light using a Syngene Bio Imaging system and the digital image was viewed with Gene Flash software™.

2.6. Restriction enzyme inhibition assay

The restriction enzyme inhibitory activity was determined by observing the resultant band of lambda (λ) DNA. Each reaction mixture contained 0.25 μg of λ DNA, 2 μl of 10× restriction enzyme reaction buffer, 50 μM of 1 or 2, 5 units of restriction enzyme and sterile deionized water. The total volume of each reaction was 20 μl. Firstly, λ DNA was incubated with the bismuth compound at 37 °C for 60 min followed by addition of the restriction enzyme. The reaction mixture was incubated for a further 2 h at the same temperature. The reactions were terminated by the addition of 2 μl of 10% SDS, followed by 3 μl of a dye solution comprising 0.02% bromophenol blue and 50% glycerol. SDS is required to denature the restriction enzyme, preventing further functional enzymatic activity. The mixtures were applied to a 2.0% agarose gel and subjected to electrophoresis for 2 h at 80 V with running buffer of TAE. The gel was stained, destained, and photographed under UV light using a Syngene Bio Imaging system and the digital image was viewed with Gene Flash software™.

2.7. Extraction of RNA, and RT^2 profiler PCR microarray (apoptosis and cell cycle analysis)

The HepG2 cells were plated at a density of 3×10^6 cells per T-75 cm^2 flask. Total RNA was extracted from cultured HepG2 cells using a high-purity RNeasy Mini Kit (Qiagen, USA) according to the manufacturer's protocols. Total RNA samples were dissolved in diethylpyrocarbonate-treated water and their concentration and quality were analyzed by electrophoresis and by UV/visible (UV/vis) spectroscopy on a BioPhotometer Spectrophotometer UV/VIS (Eppendorf, Germany).

The real-time PCR microarray assay was performed using the RT^2 Profiler PCR microarray (Apoptosis (PHAS-012); cell cycle (PHAS-020)) according to the manufacturer's protocols (Qiagen, Germany). The human apoptosis RT^2 profiler PCR array profiles the expression of 84 key genes involved in programmed cell death. This array contains genes that both positively and negatively regulate the cell cycle, the transitions between each of the phases, DNA replication, checkpoints and arrest. Gene expression was compared according to the CT value.

2.8. Caspase activity (caspases 3, 7, 8, 9 and 10)

Caspase activity was assayed by measuring the light intensity using a kit (Caspase Assay, Milipore) and a luminometer (Perkin Elmer HTS 7000, France). Briefly, cells were cultured in 96-well plates in a final volume of 200 mL. Then 50 mL caspase reaction buffer was added and incubated at room temperature for 1 h before measurement.

2.9. Intracellular reactive oxygen species (ROS) measurements

5-(And-6)-carboxy-2′,7′-dichlorodihydrofluorescein diacetate (Carboxy-H2DCFDA, Sigma, USA) was used to detect intracellular ROS according to the manufacturer's instructions. For ROS quantification, cells were seeded in 96-well black plates (Greiner Bio-One, France) and treated with 1 or 2 at the indicated IC_{50} concentrations for 24 h. Afterwards, the cells were washed with PBS and incubated with 10 μM carboxy-H2DCFDA in DPBS for 1 h. The cells were then washed and fluorescence measured by a plate reader (Perkin Elmer, France) with an excitation wavelength of 485 nm and an emission wavelength of 535 nm.

2.10. Flow cytometry analysis (fluorescence-activated cell-sorting)

The HepG2 cells were plated at 1×10^6 cells per T-75 cm^2 flask. The cells were maintained in a medium supplemented with 0.53 μM (1) and 55.9 μM (2) in DMSO for the treated cells. A control was performed with DMSO alone. The cells were collected after 6, 12 and 24 h. The cells were harvested, fixed in 70% ethanol and stored at −20 °C. Cells were then washed twice with ice-cold PBS and incubated with RNase and the DNA intercalating dye PI. Cell-cycle phase analysis was performed using a Becton Dickinson Facstar flow cytometer equipped with Becton Dickinson cell-fit software™.

2.11. Cytochrome c detection

The HepG2 cells were plated at 1×10^6 cells per T-75 cm^2 flask. The cells were maintained in a medium supplemented with 0.53 μM (1) and 55.9 μM (2) in 1% DMSO for the treated cells. A control was performed with 1% DMSO alone. Cytochrome c was detected by FlowCellect™ Cytochrome C Kit (Millipore, Germany) according to the manufacturer's protocol (http://www.millipore.com/catalogue/item/fcch100110#).

2.12. Cell invasion assay

The cell invasion study was conducted employing a BioCoat™ Matrigel™ Invasion Chamber (BD Biosciences, San Jose, CA). Briefly, 0.75 ml of complete medium was added to the bottom of the well. At the same time, 5×10^4 cells, re-suspended in 0.5 ml complete medium with or without compound 1 and 2 (0.53 μM and 55.9 μM, respectively), were added to the insert of the well. The final concentration of DMSO was identical in all the inserts (0.01%). The cells were then incubated at 37 °C under 5% CO_2 for 22 h. Non-invaded cells in the interior of the insert were removed with cotton tips. Invaded cells were fixed with methanol for 2 min, followed by staining with 1% Toluidine Blue O (Sigma-Aldrich) and washing with water. The membrane was finally observed under an inverted microscope at 200× magnification. Ten fields were randomly chosen and the numbers of invaded cells were counted. The data are shown mean ± SEM from three independent experiments.

3. Results

3.1. Chemistry

Compounds 1 and 2, Fig. 1, exhibited the expected spectroscopic characteristics (see Section 2.2) confirming their formation. Crystal structures are known for each of 1 [24] and 2 [25] and feature anisobidentate coordination of the dithiocarbamate ligands and heavily distorted geometries owing to the presence of a stereochemically active lone pair of electrons coupled with secondary Bi…S interactions. PXRD measured on the samples prepared herein matched those calculated

from the respective single crystal studies; see Fig. S1. This indicates that the bulk material has the same structure as determined by single crystal X-ray crystallography. Time-dependent ^{1}H NMR measurements in DMSO-d6 on each of 1 and 2 showed no change after 36 h, indicating their stability beyond the time-frame of the biological studies described below.

3.2. Inhibition of cancer cell proliferation

Compounds 1 and 2 were evaluated in vitro for their ability to inhibit cell proliferation against six human cancer lines, i.e. HepG2, MCF-7R, A2780, HT-29, A549 and thyroid 8505C, with cisplatin, doxorubicin and paclitaxel as the positive controls. The effects of the compounds on the growth and proliferation of the selected cell lines were evaluated after 24 h and the obtained IC_{50} values are listed in Table 1. Generally, 2 was non-potent, only exhibiting limited potency against HepG2. By contrast, 1 was more cytotoxic than any of the standard drugs in all the investigated cell lines. The viability of the HepG2 cells after treatment with 1 and 2 at different concentrations is plotted in Fig. 2 which shows that 1 and 2 inhibited cell proliferation in a concentration-dependent manner. HepG2 was selected for the subsequent studies into mechanisms of cell death.

3.3. Membrane permeability study (AO/PI apoptotic cell study)

The assessment of the membrane integrity of the HepG2 cells after treatment with the respective IC_{50} dose of each compound was accomplished by staining with AO/PI as shown in Fig. 3. Apoptotic cells exhibit increased plasma membrane permeability to certain fluorescent dyes [26]. In this assay, cells with an intact membrane appear to have a bright-green nucleus while apoptotic cells exhibit a dark-green nucleus with condensation of chromatin (as dense-green areas) when viewed by fluorescence microscopy after being stained with AO [27]. Necrotic cells on the other hand have lost membrane integrity and show bright-red fluorescence with PI as this is impermeable to intact plasma membranes but can easily penetrate the plasma membrane of dead or dying cells to intercalate with DNA or RNA thereby producing a bright-red fluorescence [28]. The AO/PI staining showed that majority of HepG2 cells underwent apoptosis after treatment with 1 and 2. Some morphological characteristics of apoptotic cells was observed on the treated HepG2 cells, such as condensation of nuclear chromatin and cytoplasm, membrane blobbing and the formation of apoptotic bodies. Some of the 1-treated cells exhibited enlargement of cell volume and formation of multinucleated cells. After treatment with 1 and 2, the majority of cells were clumped in few unorganised colonies (Fig. 3b,c), while this phenomenon was not shown for the untreated cells (Fig. 3d). Furthermore, a small amount of red fluorescence appears in most of the 2-treated apoptotic cells with intact plasma membrane, Fig. 3c, indicating that 2 might also trigger cell necrosis at the same time.

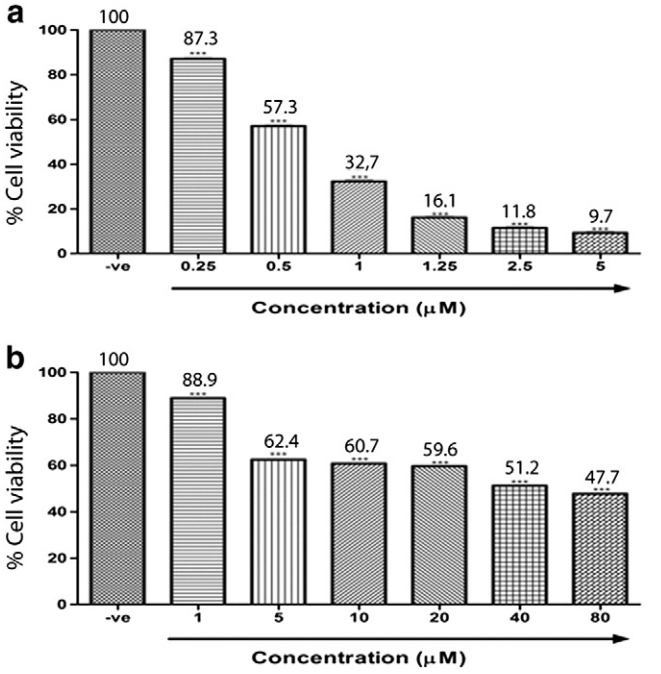

Fig. 2. (a) 1 and (b) 2. Cell viability of HepG2 cells after treatment with 1 and 2 at different concentrations at 24 h.

3.4. DNA fragmentation analysis

Chromosomal DNA fragmentation is one of the hallmarks of the lethal stages of apoptosis that proceeds in a two-step manner. At first, the DNA is initially cleaved into 50–300 kb fragments and eventually into oligonucleosomal pieces [29,30]. The release of apoptotic signals during the apoptosis process such as the expression of the p53 and DFFA genes leads to DNA damage. As shown in Fig. 4 (L2, L4), 1 and 2 causes intensified DNA fragmentation in HepG2 cells noticeable by the generation of ladder fragments in individual cells resulting from DNA breaks (shown by arrows).

3.5. Restriction enzyme digestion and analysis

The sequence binding selectivity of 1 and 2 to DNA was studied in detail by measuring the inhibition of twelve different restriction enzymes which differ in their target sequences. The list of restriction enzymes and their target sequences (red arrows) are as follows:

1.	Tsp 509I	5′-↓ A A T T-3′ 3′-T T A A ↑-5′
2.	Hae III	5′-G C ↓G C-3′ 3′-C G ↑C G-5′
3.	Sal I	5′-G ↓T C G A C-3′ 3′-C A G C T ↑G-5′
4.	Pst I	5′-C T G C A ↓G-3′ 3′-G↑ A C G T C-5′
5.	Pvu II	5′-C A G ↓C T G-3′ 3′-G T C ↑ G A C-5′
6.	Sca I	5′-A G T ↓A C T-3′ 3′-T C A ↑ T G A-5′
7.	Ssp I	5′-A A ↓T A T T-3′ 3′-T T A T ↑A A-5′
8.	Ase I	5′-A T ↓T A A T-3′ 3′-T A A T ↑T A-5′
9.	Mun I	5′-C↓ A A T T G-3′ 3′-G T T A A ↑C-5′

(continued on next page)

Table 1
Cytotoxic activity of 1, 2 and standard drugs against human carcinoma cells after 24 h treatment.[a]

	Cisplatin	Doxorubicin	Paclitaxel	1	2
Cell line	IC_{50} (μM)	IC_{50} (μM)	IC_{50} (μM)	IC_{50} (μM)	IC_{50} (μM)
HepG2	152.0 ± 0.3	4.6 ± 0.2	>80	0.5 ± 0.4	55.9 ± 0.3
MCF-7R	19.6 ± 0.2	5.2 ± 0.4	15.9 ± 0.3	0.9 ± 0.2	>80
A2780	28.8 ± 0.4	4.4 ± 0.2	14.2 ± 0.3	0.5 ± 0.2	>80
HT-29	25.0 ± 0.3	4.8 ± 0.3	>80	3.5 ± 0.3	>80
A549	35.4 ± 0.4	>80	>80	2.3 ± 0.4	>80
8505C	120.0 ± 0.2	>80	>80	0.2 ± 0.4	>80

[a] Means and standard deviations from at least two independent experiments conducted in triplicate, except for values >80.

(*continued*)

10.	EcoR I	5′-G↓ A A T T C-3′ 3′-C T T A A ↑G-5′
11.	Nde I	5′-C A↓ T A T G-3′ 3′-G T A T ↑A C-5′
12.	Bst 11071	5′-G T A ↓ T A C-3′ 3′-C A T ↑ A T G-5′

The twelve restriction enzymes were used to assess the binding selectivity of 1 and 2 towards λ DNA as anti-cancer activity can be manipulated when specific binding occurs with DNA, either by intercalation or via groove binding. Gel electrophoresis following the digestion with the twelve restriction enzymes of λ DNA pre-treated with 1 and 2 is illustrated in Figs. 5 and 6; precise and reproducible protection patterns were observed for each DNA interaction study. Based on the results, the 'AT' sequence in Ssp I "AATATT", Nde I "CATATG" and Bst 11071 "GTATAC" was sheltered from DNase digestion by 1, whereas the GC, short AT, AAT and random sequences were not. These conclusions are based on the fact that digestion with Ssp I, Nde I and Bst 11071 did not induce DNA scission on the λ DNA suggesting that 1 was bound to specific DNA sites and protects these from restriction enzymes digestion [31] while digested DNA bands were shown in the negative control (Figs. 5a, 6a). Conversely, 2 failed to protect the restriction sites in any of the twelve tested restriction enzymes as discerned from the bands appearing in the gel which correspond to the restriction sites of the enzyme (Figs. 5B, 6B).

3.6. Intracellular signalling cascades

Apoptosis is a highly controlled process of programmed cell death for eliminating unwanted cells from the body during organ development, immune responses and tissue remodelling. The resistance of tumours to chemotherapy has been closely related to the inherent weaknesses in apoptotic pathways in the development of cancer. Hence, numerous anti-cancer drugs are aimed specifically at the signalling components of cell death and survival pathways [32–34]. In general, apoptosis is characterised by an individual set of biochemical stages and morphological changes comprising chromatin condensation, activation of caspases and chromosomal DNA fragmentation [35].

Cell death pathways affected by 1 and 2 were evaluated by a combination of apoptosis RT^2 profiler PCR microarray analysis, caspase activity study, DNA fragmentation and ROS production measurements. The proposed signalling pathways are summarised in Fig. 7. Over-expression of pro-apoptotic genes accompanied by suppression of anti-apoptotic

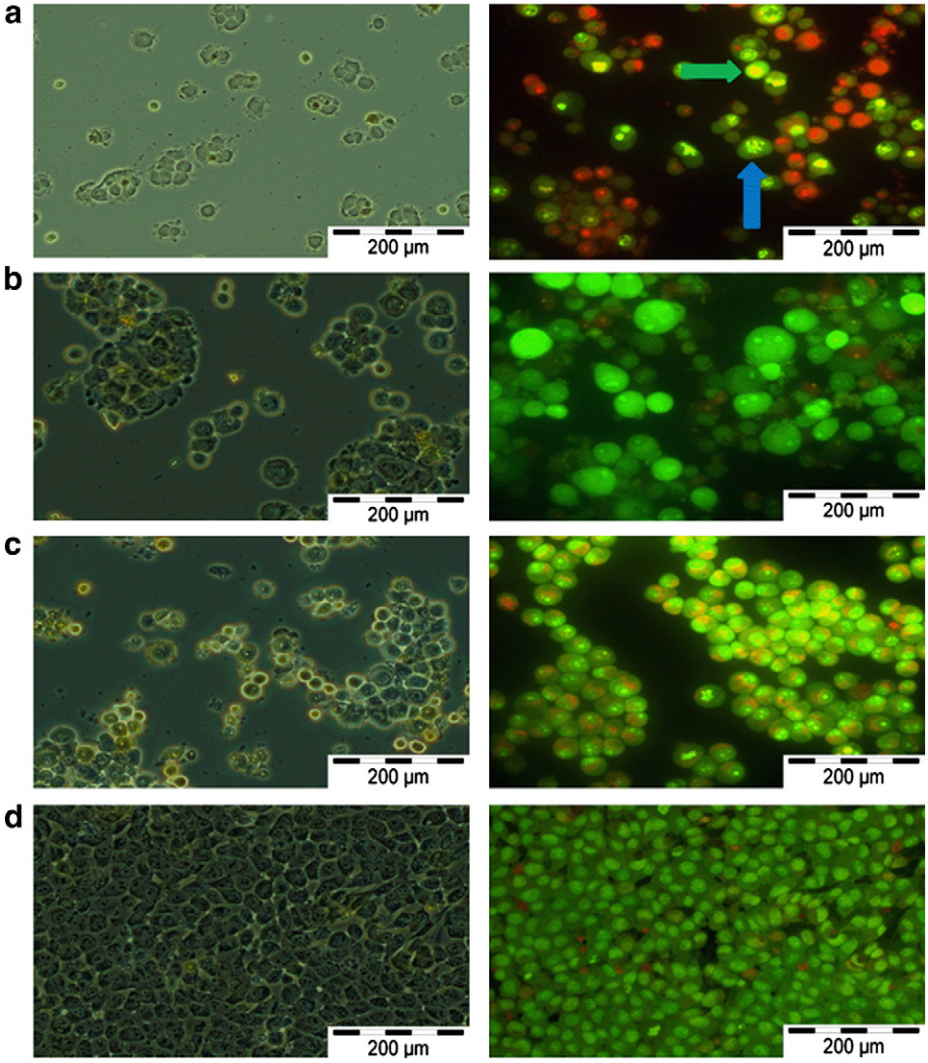

Fig. 3. AOPI staining of HepG2 cells after being treated with the IC_{50} value of each compound. (a) doxorubicin; (b) 1; (c) 2; (d) untreated cells (negative control). The red colour was produced by the PI stain which penetrated the nuclear matter when the cell membrane integrity was disturbed. Cells with intact membrane are stained green. Apoptotic cells are stained dark-green and contain multiple yellow/green dots of condensed nuclei. Necrotic cells were stained bright-red due to the influx of PI stain. The green arrow in (a) shows a healthy cell. The blue arrow in (a) shows an apoptotic cell with fragmented nucleus and condensed chromatin. Magnification = 100×.

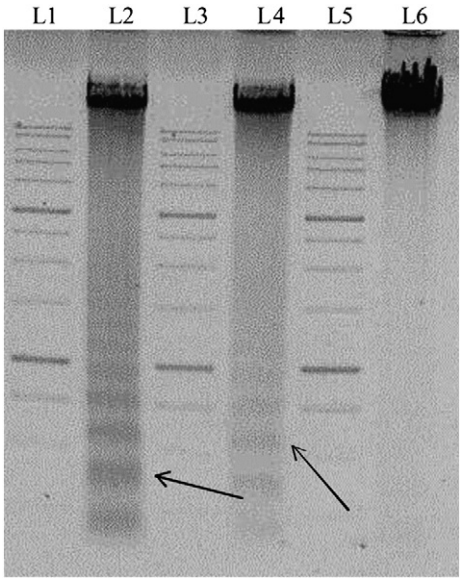

Fig. 4. DNA fragmentation analysis. The HepG2 cells were cultured for 24 h in RPMI 1640 in the presence of 0.53 μM 1 (L2) and 55.9 μM 2 (L4). DNA was extracted from the cultures and DNA fragmentation was detected using an electrophoresis system with a 2% agarose gel. L1, L3 and L5 are 1 kb DNA ladder; L6 is negative control (untreated cells). Formation of ladders on the gel to indicate DNA fragmentation occurs following treatment with 1 and 2 (indicated by arrows) which suggests that cell death is by apoptosis.

genes was observed following the treatment of HepG2 with 1 and 2. This work provides evidence that the cytotoxicity of 1 and 2 is related to the induction of a p53/p73-dependent activation of the mitochondrial pathway of apoptosis, demonstrating the anti-cancer properties of the compounds. Interestingly, the PCR microarray analysis revealed that 1 induced apoptosis involving both intrinsic and extrinsic pathways mediated by various types of apoptosis-inducing factors. Both p53 and p73 were expressed at the same time. Compounds 1 and 2 were found to trigger the gene expression of p53 (TP53 gene) as seen by about a 6- and 10-fold increase over TP73 expression (Table 2). The up-regulation of the p53/p73 genes shows that the compounds could induce DNA damage in HepG2 cells, which is consistent with the DNA fragmentation results discussed above (see Section 3.4 and Fig. 4). At the same time, the p21 encoded gene, CDKN1A, that functions as a major inhibitor of p53-dependent apoptosis [36], was up-regulated by 1 and 2, 12- and 22-fold (after 24 h), respectively (Fig. 8). Another upstream protein that regulates p53 is the ataxia telangiectasia mutated (ATM) gene that was up-regulated by 1 and 2 about 98- and 21-fold (after 24 h), respectively (Fig. 8). The ATM gene initiates a mechanism for controlling cell cycle and apoptotic responses by selectively stimulating the expression of p53 [37], so the up-regulation of CDKN1A gene and the up-regulation of the ATM gene work against each other in the enhancement of the p53 pathway.

It is noted that the level of gene expression of ATM by 1 is significantly greater than promoted by 2 which may be one of the reasons why 1 has greater cytotoxicity than 2. The enhancement of p73-induced apoptosis after treatment with 1 and 2 is due to the presence of c-Abl protein which also leads to the inception of apoptosis [38] (Table 2; ABL1 gene). The high expression of the BNIP3L protein, a cell death inducer, in 1- and 2-treated cells (55- and 23-fold) by p53 is considered as supportive evidence for the activation of the p53 gene as this can directly up-regulate the expression of the BNIP3L gene which is known to be highly induced in wild-type p53-expressing cells [39].

The BCL-2-associated X protein (BAX) initiates a second mechanism of p53/p73-induced apoptosis, which in turn promotes Bax mitochondrial translocation and cytochrome c release. In general, mitochondrial membrane permeability is controlled through a family of proto-oncogenes, such as anti-apoptotic (BCL-2) and pro-apoptotic (BAD, BAX) [40]. BAX is introduced into the mitochondrial membrane and increases membrane permeability, thereby promoting apoptosis once activated [41,42]. In the treated HepG2 cells, BCL-2 was deactivated by 1 and 2 (Table 2), hence, BAX is able to increase mitochondrial membrane potential without obstruction in the absence of anti-apoptotic protein, BCL-2.

Generally, the primary event leading to apoptosis is the loss of mitochondrial trans-membrane potential [43] which results in the compromise of the $\Delta\Psi m$, followed by outer mitochondrial membrane disruption and release of proteins such as the cytochrome c from the inter-

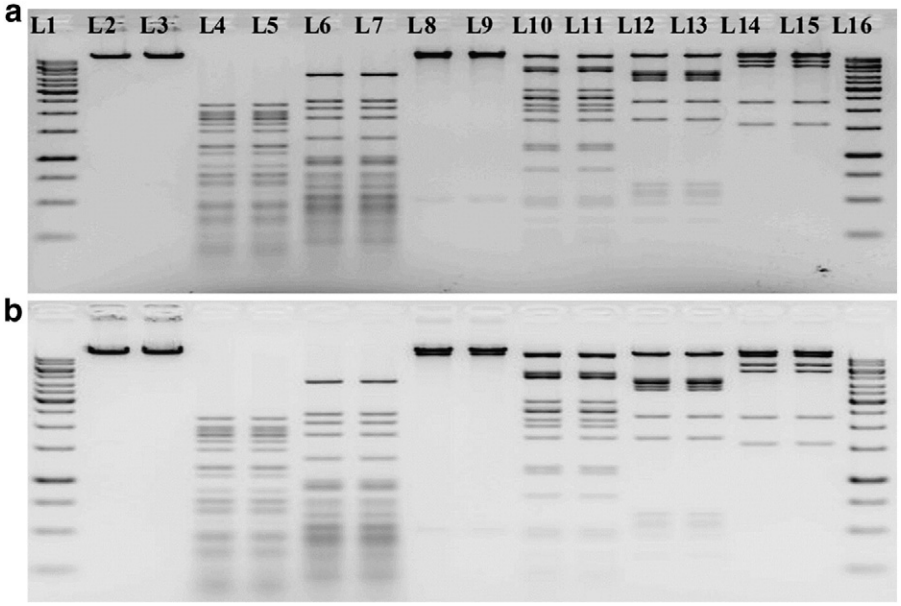

Fig. 5. Electrophoresis results after incubating λ DNA (0.5 μg/μL) with 5 units of restriction enzyme in the presence or absence of 10 μM 1 (a) and 2 (b) for 2 h at 37 °C. Lanes 1 and 16, 1 kb DNA ladder; Lane 2, λ DNA alone (0.5 μg); Lane 3, λ DNA + 10 μM compound; Lane 4, λ DNA + 5 units Tsp 509I (control); Lane 5, λ DNA + 5 units Tsp 509I + 10 μM compound; Lane 6, λ DNA + 5 units Hae III (control); Lane 7, λ DNA + 5 units Hae III + 10 μM compound; Lane 8, λ DNA + 5 units Sal I (control); Lane 9, λ DNA + 5 units Sal I + 10 μM compound; Lane 10, λ DNA + 5 units Pst I (control); Lane 11, λ DNA + 5 units Pst I + 10 μM compound; Lane 12, λ DNA + 5 units Pvu II (control); Lane 13, λ DNA + 5 units Pvu II + 10 μM compound; Lane 14, λ DNA + 5 units Sca I (control); and Lane 15, λ DNA + 5 units Sca I + 10 μM compound.

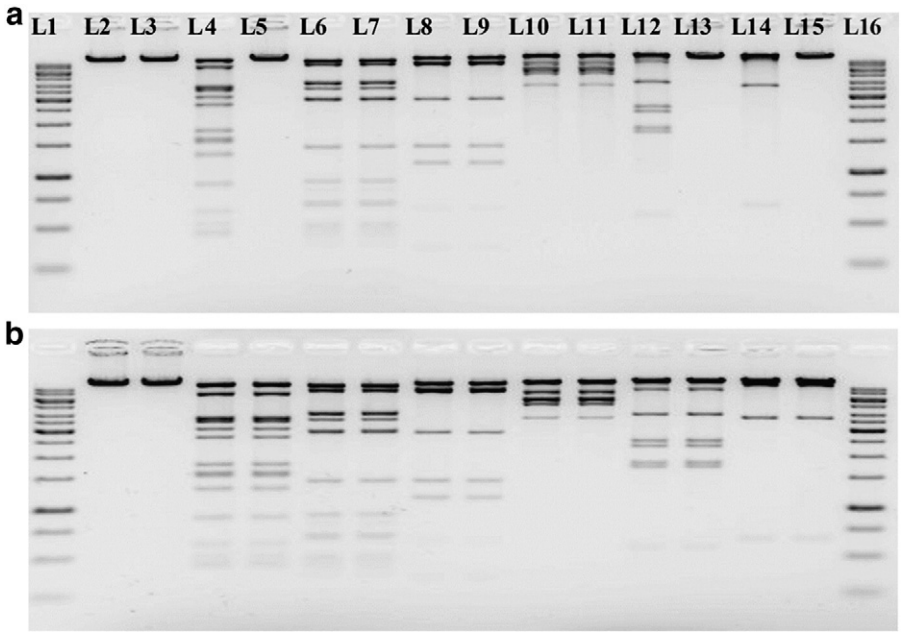

Fig. 6. Electrophoresis results after incubating λ DNA (0.5 μg/μL) with 5 units of restriction enzyme in the presence or absence of 10 μM 1 (a) 2 (b) for 2 h at 37 °C. Lanes 1 and 16, 1 kb DNA ladder; Lane 2, λ DNA alone (0.5 μg); Lane 3, λ DNA + compound; Lane 4, λ DNA + 5 units Ssp I (control); Lane 5, λ DNA + 5 units Ssp I + compound; Lane 6, λ DNA + 5 units Ase I (control); Lane 7, λ DNA + 5 units Ase I + compound; Lane 8, λ DNA + 5 units Mun I (control); Lane 9, λ DNA + 5 units Mun I + compound; Lane 10, λ DNA + 5 units EcoR I (control); Lane 11, λ DNA + 5 units EcoR I + compound; Lane 12, λ DNA + 5 units Nde I (control); Lane 13, λ DNA + 5 units Nde I + compound; Lane 14, λ DNA + 5 units Bst 11071 (control); and Lane 15, λ DNA + 5 units Bst 11071 + compound.

membrane region [44]. Cytochrome c, which binds to apoptotic activating factor-1 (APAF-1), was also significantly expressed in HepG2 cells treated with 1 and 2, and is known to activate caspase-9 leading in turn to the activation of caspase-3 which is the most potent effector caspase (Table 2). The increase in $\Delta\Psi m$ also allows for the release of AIF, which activates a DNase leading to apoptosis [45-47]. Downward shifts (from M2 to M1) in the fluorescence response due to cytochrome c in HepG2 cells after treatment of 1 and 2 after 12 and 24 h are illustrated in Fig. 9; the negative control samples show low levels of cytochrome c loss.

Another outcome from the increase in the mitochondrial membrane potential is the generation of ROS. The generation of ROS is reportedly involved in apoptosis induced by chemotherapeutic agents through the activation of the mitochondria-mediated apoptotic pathways [48,49]. ROS are thought to play a role in TNFR (tumour necrosis factor receptor) and FAS (tumour necrosis factor superfamily, member 6) receptor-mediated apoptosis even though the exact mechanism remains undefined [50]. In the presence of 1 and 2, cellular ROS generation exceeded about 32% and 21% that of the negative control (untreated cells), indicating that the trial compounds do induce significant H_2O_2 generation (Fig. 10). These findings suggest that 1 and 2 activate the intrinsic pathway by enhancing ROS production and repressing mitochondrial function, and contributes to apoptotic cell death in HepG2 cells. Drugs which are able to compromise the functional integrity of mitochondria could be of significant relevance in anti-cancer therapy [51].

The present study revealed that treatment of HepG2 cells with 1 and 2 also induced an extrinsic apoptotic pathway by triggering death

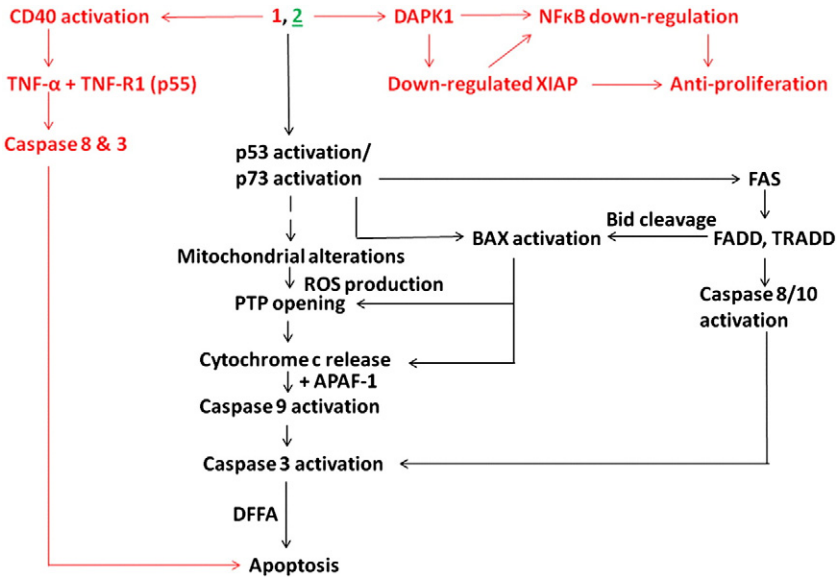

Fig. 7. Proposed signalling pathway of apoptosis induced by 1 and 2. This diagram represents a collation of the results obtained from the PCR microarray analysis, caspase activity study, DNA fragmentation and ROS production measurements.

Table 2
Apoptosis gene expression level in HepG2 cell lines after treatment with 1 and 2 compared to untreated cells.[a]

	Up–down regulation fold regulation (comparing to control group)	
	1	2
ABL1	**58.13**	**253.96**
AKT1	**72.06**	**241.94**
APAF1	**33.17**	**12.62**
BAD	**34.56**	**49.81**
BAG1	*−11.62*	**21.51**
BAG3	*−54.99*	**172.26**
BAG4	*−14.13*	**236.96**
BAK1	**64.50**	**164.11**
BAX	**34.99**	**14.04**
BCL10	**11.64**	**26.51**
BCL2	*−16.63*	*−6.33*
BCL2A1	**9.59**	**18.75**
BCL2L1	*−5.70*	**61.33**
BCL2L10	*−8.41*	**1.01**
BCL2L11	**3.08**	**8.16**
BCL2L2	**35.54**	**123.51**
BCLAF1	**93.78**	**393.03**
BFAR	**1.55**	**2.88**
BID	**13.37**	**2.16**
BIK	**7.52**	**8.22**
NAIP	**24.44**	**67.11**
BIRC2	*−1.35*	**1.85**
BIRC3	*−185.95*	*−30.94*
XIAP	*−68.65*	**4.90**
BIRC6	*−56.06*	*−24.28*
BIRC8	*−18417.65*	*−4842.45*
BNIP1	**75.12**	**179.58**
BNIP2	**227.73**	**595.72**
BNIP3	*−87.96*	*−49.92*
BNIP3L	**55.28**	**22.65**
BRAF	*−22.92*	*−8.18*
NOD1	**22.03**	**99.63**
CARD6	**1.01**	**1.09**
CARD8	**3.10**	**3.50**
CASP1	**44.67**	**54.51**
CASP10	**1.01**	**4.43**
CASP14	**1.01**	**33.32**
CASP2	**58.94**	**304.12**
CASP3	**97.69**	**4.91**
CASP4	**8.64**	**9.31**
CASP5	**3.41**	**3.36**
CASP6	**38.35**	**109.78**
CASP7	**27.69**	**159.62**
CASP8	**37.57**	**14.32**
CASP9	**103.34**	**160.95**
CD40	**12.33**	**1.01**
CD40LG	**8.64**	**1.01**
CFLAR	**28.47**	**46.48**
CIDEA	*−1.19*	*−1.19*
CIDEB	**23.77**	**134.22**
CRADD	**37.04**	**112.87**
DAPK1	**42.54**	**1.01**
DFFA	**103.34**	**59.16**
FADD	**7.42**	**18.23**
FAS	**42.85**	**131.46**
FASLG	**6.03**	**8.39**
GADD45A	**4.26**	**2.62**
HRK	**10.06**	**18.11**
IGF1R	*−212.13*	*−86.91*
LTA	**9.52**	**11.22**
LTBR	**215.45**	**395.76**
MCL1	**36.53**	**69.00**
NOL3	**82.21**	**160.73**
PYCARD	**1.04**	**1.01**
RIPK2	**37.82**	**180.83**
TNF	*−7.94*	*−7.95*
TNFRSF10A	**22.49**	**65.73**
TNFRSF10B	**250.94**	**928.32**
TNFRSF11B	**6.28**	**20.80**
TNFRSF1A	**138.26**	**225.73**
TNFRSF21	**12.65**	**51.57**
TNFRSF25	**1.01**	**93.60**
CD27	*−1.88*	*−1.32*
TNFRSF9	**1.01**	**1.01**
TNFSF10	**2.95**	**2.03**
CD70	**2.93**	**3.29**
TNFSF8	**7.47**	**5.42**
TP53	**113.08**	**90.63**
TP53BP2	**4.41**	**22.76**
TP73	**18.79**	**8.62**
TRADD	**35.29**	**92.31**
TRAF2	*−1.05*	**77.11**
TRAF3	*−3.14*	**73.46**
TRAF4	*−11.74*	**51.98**

Bold face: up-regulated genes; italic: down-regulated genes.
[a] Data represent mean of samples 1 and 2-induced fold-change in gene expression relative to control-treated cells ($n = 3$), $p < 0.05$.

receptors of the tumour necrosis factor receptor superfamily, member 6 (FAS) and the tumour necrosis factor receptor (TNFRSF1A) gene expression. Caspases-8, -10, -9 and -3 were activated subsequently after FAS expression with an increase in their enzymatic activities (Tables 2–4). In general, FAS and TNFR1 recruit Fas-associated protein with death domain (FADD) and procaspase-8 and -10 to the receptor. FADD controls the recruiting of procaspase-8 and -10 leading to its auto-cleavage and activation, and subsequently activates effector caspases in initiating cell death [52,53]. Alternatively, caspase-8 and -10 could cleave the BCL-2 family member Bid, a molecular linker bridging death receptor and mitochondria pathways to truncated BH3 interacting-domain death agonist (tBID), that binds to pro-apoptotic protein BAX, resulting in the disruption of mitochondrial membrane potential and the release of cytochrome c [54–56]. Compounds 1 and 2 also induced expression of BID in HepG2 cells (Table 2), which provides additional supporting evidence for the proposed apoptotic pathways.

Interestingly, apart from the mitochondrial and FAS death receptor apoptotic pathway, 1 was also found to induce another death receptor-dependent pathway by induction of a series of pro-apoptotic genes, such as CD40 (CD40 gene), CD40L (CD40LG), TNF-α (TNF) and TNF-R1 (p55/TNFRSF1A) (Table 2). CD40 is a TNF receptor family member that is widely recognized for its prominent role in immune regulation and homeostasis [57]. However, accumulating evidence suggests that the CD40 pathway can be exploited for cancer therapy as it can stimulate the host's anti-tumour immune response, followed by normalisation of the tumour microenvironment and arrest of the growth of CD40-positive tumours [57]. Further, CD40 also contains a cytoplasmic motif reminiscent of the death domain which is involved in the initiation of TNF-R1 and CD95-dependent apoptosis, stimulating cell death in cells of mesenchyme origin, tumour cells and certain transformed cell lines [58–60]. Moreover, membrane- anchored TNF-α and TNF-R1 (p55) may be activated by CD40 followed by stimulation of the death receptor-dependent pathway involving caspases-8 and -3 [61].

In another pathway, death-associated protein kinase 1 (DAPK1), a tumour suppressor, was highly expressed by 1 in HepG2 cells (by about 43-fold; Table 2). Over-expression of siDAPK1 significantly rescues the protein expression of transcription factor Rel/nuclear factor-kappaB (NF-κB)-targeted genes [62]. NF- B plays a crucial role in regulating gene transcription and is involved in the mechanism of cell proliferation [63,64]. DAPK1 also suppresses protein expression of anti-proliferation genes such as COX-2 and ICAM-1, and anti-apoptosis genes such as XIAP, which is involved in apoptosis inhibition triggered by multiple varied stimuli that activate both of the principle cell death pathways [65]. XIAP is an efficient apoptotic inhibitor because it is critically positioned to act at the point of convergence of both the extrinsic

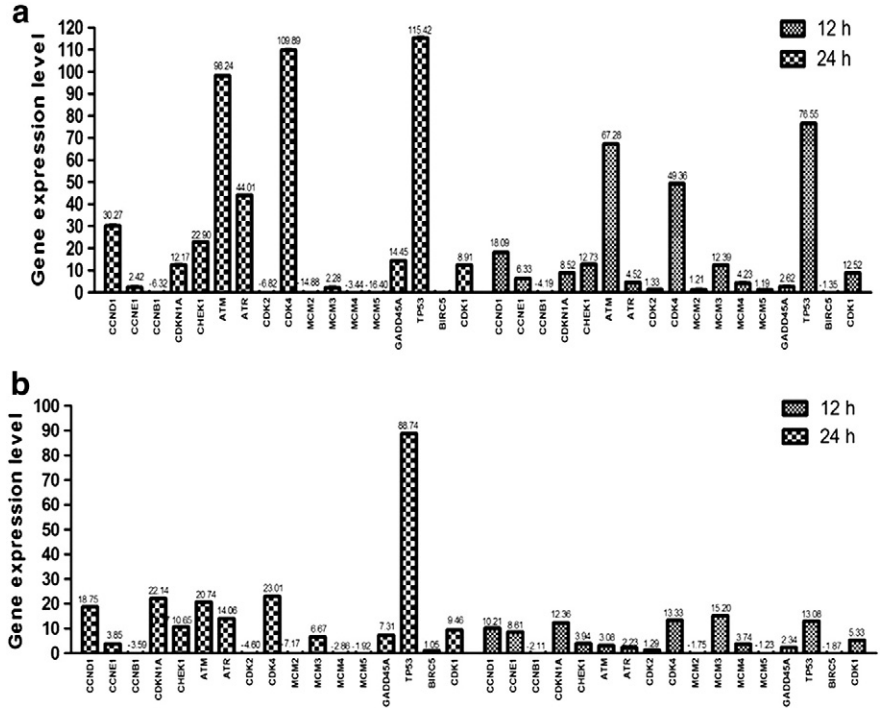

Fig. 8. Cell cycle gene expression level in HepG2 cell lines after treatment with compound 1 (a) and 2 (b) at 12 and 24 h compared to untreated cells corresponding to value 1. *$p < 0.05$.

and intrinsic death pathways on effector caspase activation [66]. Likewise, XIAP directly obstructs the activities of multiple caspases, particularly, the effector caspases-3, -7 and -9 either by direct enzyme inhibition or through ubiquitin-mediated proteasome degradation [66]. XIAP is highly expressed in many cancer cells and tumour specimens. Therefore, its inactivation in cancer cells results in apoptosis [67,68]. In the present investigation, XIAP was significantly down-regulated by 1 after 24 h of incubation in HepG2 cells (Table 2). Under the same conditions, 2 induced high expression of XIAP (5-fold) which defers the cell death process in HepG2 cells. Furthermore, over-expression of XIAP will cause cancer progression and increase the resistance-level of cancer cell lines to chemotherapy [67,68].

3.7. Cell cycle analysis

The cell cycle is a fundamental process that is studied in order to comprehend the mechanisms of tumour growth. In the realm of metal-based compounds, several gold compounds have been reported to exhibit anti-cancer activities through the modulation of the cell cycle and the inhibition of the growth of cancer cells [69,70]. In this study, HepG2 cells were treated with 1 and 2 for various time periods (6, 12, and 24 h) to determine whether the growth-inhibitory effect was associated with the induction of cell cycle arrest and/or apoptosis; the distribution of cells in the different phases of the cell cycle was analyzed using flow cytometry. Both 1 and 2 inhibited the growth of HepG2 cancer cells via cell cycle arrest at the S and G_2/M phases. The accumulation of cells in the S and G_2/M phases was accompanied by synchronous decreases in the percentage of cells in the G_0/G_1 phase in a time-dependent manner up to 24 h (Figs. 11 and 12). Significant changes in the population of cells in the G1 phase or in the levels of proteins related to G_1 phase, such as Ckd4, were observed (Fig. 8). Further, the exposure of 1 and 2 was associated with cellular phenotypic changes, such as cell shrinkage and density (Fig. 3b,c).

Cell cycle arrest and apoptosis progression are the main machineries involved in anti-cancer drug treatment [71,72]. In recent studies, certain anti-cancer agents induced cell cycle G1 arrest and decreased cyclin D_1 and/or cyclin E expression in cancer cells [73,74]. In the present study, cell cycle analysis revealed a prominent S and G_2/M arrest of HepG2 cells upon exposure to 1 and 2, and increases cyclin D_1 ($CCND_1$), and cyclin E ($CCNE_1$) gene expression at 24 h after the treatment (Fig. 8), suggesting that the reduction of cyclin D_1 and cyclin E, mediates the S phase cell cycle arrest by regulating the indispensable S phase passage.

Cdc2 (CDK1) interacts with cyclin B1 (CCNB1) and forms a cdc2-cyclin B_1 complex. Generally, inactivation of the cdc2-cyclin B_1 complex inhibits the transition from the G2 to M phase as this complex plays a crucial role in G_2/M phase regulation [75]. The M-phase inducer phosphatase 3, cdc25c, plays an important role in the dephosphorylation of cdc2, and the activation of cdc25c brings the subsequent activation of the cdc2-cyclin B_1 complex [76]. In addition, cyclin-dependent kinase inhibitor p21 (CDKN1A), regulates cell cycle progression. Notably, the level of expression p21 increased at the G_2/M transitions in a variety of cancer cells [77–80]. The anti-cancer effect in HepG2 cells exhibited by 1 and 2 was partially associated with their capacity to trigger growth inhibition at the G_2/M phase by down-regulation of gene expression of cdc2, cyclin B_1 and p21 (Fig. 8 and Table 2).

ATM and Rad3-related protein (ATR) are two protein kinases of the PI-3 PIKK family that activate signalling networks to freeze cell cycle progression followed by termination of DNA replication and initiation of DNA damage. The serine/threonine-protein kinase (Chek1) is an enzyme that in humans is encoded by the CHEK1 gene is a downstream effecter of ATR and ATM, and is crucial for mediating G2/M arrest following double-strand breaks [81,82]. In response to replication stress, Chek1 delays both mitotic entry and S-phase replication delays mitotic entry, and stabilizes stalled replication forks [83]. In this study, CHEK1 was significantly up-regulated by 1 and 2, approximately 23- and 11-fold, respectively, after incubation for 24 h, together with up-regulation of ATR and ATM (Fig. 8). These results are corroborated with the flow cytometry analysis, in which 1 induced approximately 24% of cell cycle arrest at the G_2/M checkpoint while the comparable value for 2 is 18% (Fig. 12).

Studies have shown that mini-chromosome maintenance (MCM) proteins of which there are six (MCM2–7), might be useful as proliferation markers in various types of cancer [84]. Generally, MCM proteins are a family of six highly conserved and highly homologous proteins

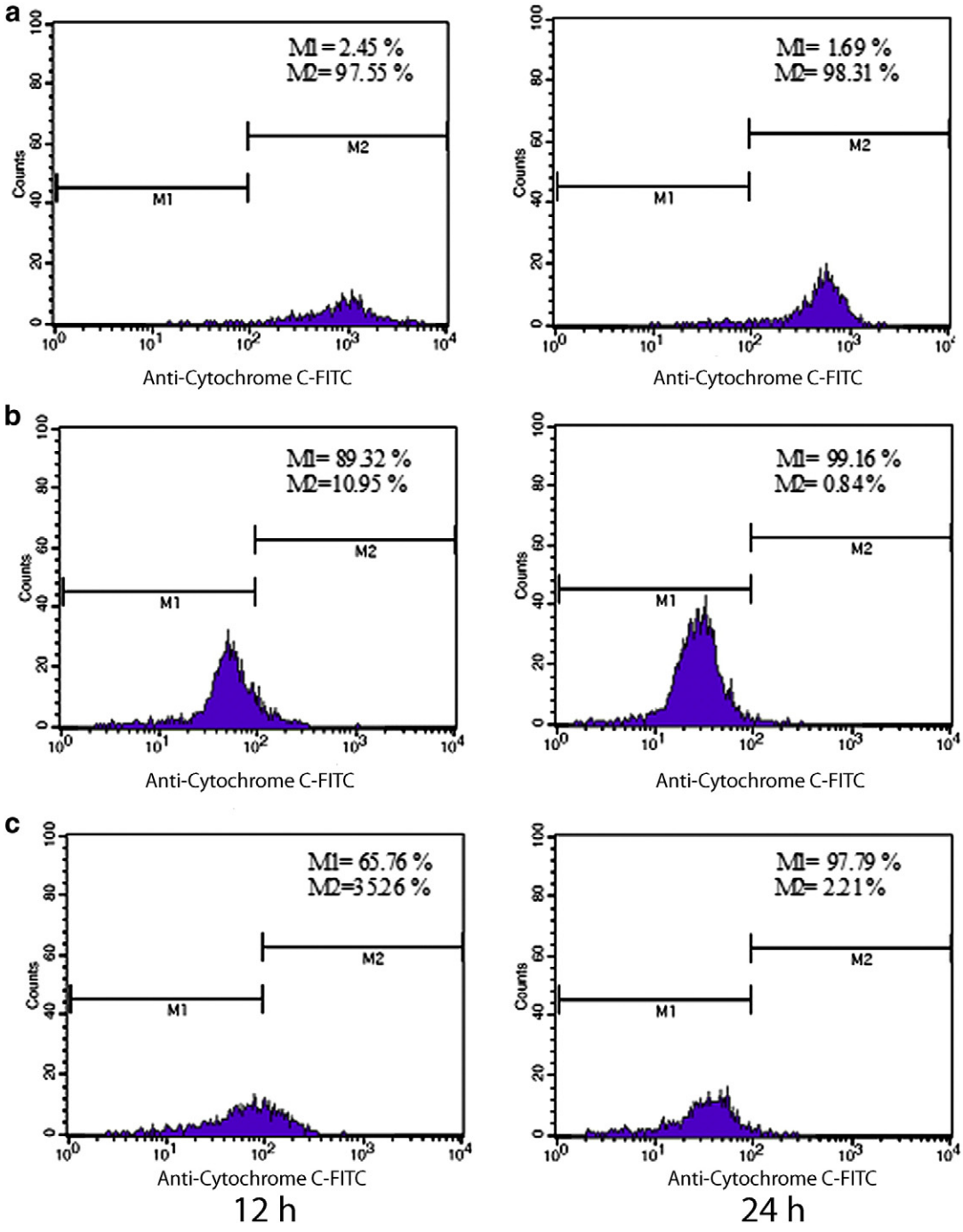

Fig. 9. Histograms depicting cells stained using the FlowCellect Cytochrome c Kit™. (a) untreated HepG2 cells after 12 and 24 h (negative control). (b) HepG2 cells treated with 0.53 μM 1 for 12 and 24 h. (c) HepG2 cells treated with 55.9 μM 2 for 12 and 24 h. (B) and (C) show downward shifts (from M2 to M1) in the fluorescence due to reduced levels of cytochrome c. Negative control samples show low levels of cytochrome c loss.

that are indispensable in forming pre-replication complexes which are responsible for allowing DNA replication [85]. Consequently, increased expression of MCM proteins has been recognised in most pre-malignant proliferative states and solid tumours. The present study showed a down-regulation of the MCM2–5 genes after treatment with 1 and 2 (Fig. 8), and suggests that they could limit the expression of MCM proteins and could act as chemo-preventive agents.

Furthermore, recent evidence suggests that p53 may also play a crucial role in the G_2/M checkpoint [86]. Induction of GADD45 in various cancer cells leads to activation of p53 in response to DNA damage [87,88]. GADD45 was up-regulated by 1 and 2 treatment with approximately 15- and 7-fold, respectively, compared to the control (Fig. 8). Moreover, in vitro, GADD45 also efficiently destabilizes cdc2-cyclin B_1 complexes, suggesting that it may mediate Cdc2/cyclin inactivation in vivo [89].

3.8. Cell invasion study

Metastasis, the main cause of death of cancer patients, is the spread of tumour cells from a primary tumour source to other organs, and remains as one of the ultimate challenges in cancer treatment [90].

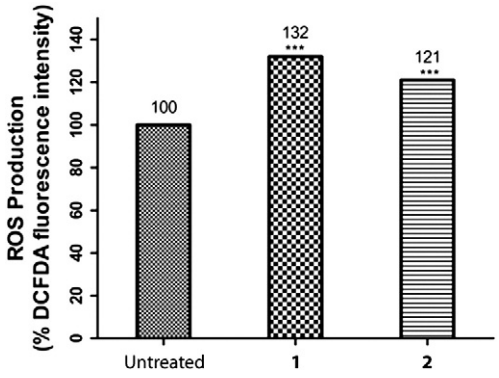

Fig. 10. Interaction of 1 and 2 with HepG2 cells recording ROS production after treatment at doses corresponding to their IC_{50} value (0.53 and 55.9 μM, respectively) for 16 h and labelled with carboxy-H2DCFDA for 1 h, after which the fluorescence response was measured.

As approaches that could prevent metastasis have not been found, the prevention of tumour metastasis is an urgent topic in cancer therapy.

An invasion assay was performed in the present study and the findings showed that 1 and 2 inhibited cell invasion. As illustrated in Fig. 13, after treatment with 1 and 2 (IC_{50} = 0.53 and 55.9 μM, respectively) the invasion rate of HepG2 cells through matrigel (*$p < 0.05$) decreased to 3.96 ± 0.52% and 40.22 ± 2.36% (normalized to 100%), respectively.

A survivin (BIRC5)-XIAP complex activates NF-κB and leads to the activation of cell motility kinases focal adhesion kinase (FAK) and c-Src tyrosine kinase (c-Src) that contribute to cancer progression and metastasis [91]. NF-κB, a heterodimeric DNA-binding protein that consists of two major subunits, p50 and p65, has been found to play a crucial role in the evolution and distant metastasis of human cancer [92–95]. Activated NF-κB can selectively bind to DNA and leads to the expression of diverse genes that regulate apoptosis, promote cell proliferation, facilitate angiogenesis, and stimulate invasion and metastasis [95,96]. However, cell migration and invasion may be increased or decreased by XIAP-deficiency in cells depending on the situation [91]. Thus, down-regulation of survivin and XIAP expression by 1 leads to the inhibition of metastasis in HepG2 cells (Fig. 13).

4. Discussion

The results from the in vitro cytotoxicity studies indicate that the IC_{50} values vary greatly between 1 and 2 in both cisplatin-sensitive and -resistant cell lines, with 1 being particularly potent and 2 generally inactive. In fact, 1 promoted significant inhibition of cell proliferation and potency levels on all tested cancer cell lines at levels comparable or greater than exhibited by cisplatin, doxorubicin and paclitaxel. These results are in accord with the original study of $Bi(S_2CNR_2)_3$ compounds which showed 1 to be the exceptionally cytotoxic against a range of cancer cells [22]; the role of the dithiocarbamate ligand is the deliver "bismuth" to the cancer cell. A qualitative structure-activity relationship was established in that cytotoxicity varied for R = Me < Et > n-Pr > n-Bu, introducing branching in R reduced cytotoxicity, and when R_2 was derived from a cyclic amine, smaller rings were more potent [22]. In the present study, it is likely that the different cytotoxicity exhibited by 1 and 2 is related to lipophilicity which is reduced for 2 owing to the presence of hydrophilic hydroxyl substituents. As both 1 and 2 exhibited significant and some activity, respectively, against HepG2, this cell line was selected for further studies.

The results of the membrane permeability study showed that the majority of HepG2 cells underwent apoptosis after treatment with both 1 and 2, but in the case of 2, some evidence was also detected for necrosis. The DNA fragmentation study was also consistent with apoptosis. Apoptopic pathways were also indicated by the experimental observations that treatment with 1 and 2 enhanced levels of cytochrome c release and ROS production.

An evaluation of the possible apoptotic pathways was conducted by quantitative PCR microarray analysis. This showed that induced apoptotic cell death involves both intrinsic and extrinsic pathways. Compounds 1 and 2 induce a p53-dependent PTP-mediated activation of the mitochondrial pathway of apoptosis in HepG2 cells allowing for the release of an apoptosis-inducing factor (AIF), which activates a DNase leading to apoptosis. The cytotoxicity of 1 was about 100-fold greater than 2, an observation that is ascribed to the observation that the caspase-3 expression by 2 is about 20 times less than that induced by 1.

Table 3
Quantification of caspases -3/7, -8 and -9 in HepG2 cells in the presence of 1 and 2.[a]

	Absorbance		
Caspase	Control	1	2
Caspase 3/7	126.0 ± 0.3	26946.0 ± 0.3	6365.0 ± 0.2
Caspase 8	135.0 ± 0.3	25782.0 ± 0.4	22018. ± 0.3
Caspase 9	130.0 ± 0.2	21805.0 ± 0.3	13085.0 ± 0.4

Means and standard deviations from four independent experiments were conducted in triplicate.
Excitation wavelength = 490 nm; Emission wavelength = 520 nm.
[a] The green fluorescent signal is a direct measure of the amount of active caspases present in the cells at the time the reagent was added.

Table 4
Quantification of AFC in HepG2 cell cultured in the presence of sample 1 and 2 upon cleavage of the AEVD-AFC substrate by caspase-10.[a]

	Absorbance		
Caspase	Control	1	2
Caspase 10	124.0 ± 0.3	1483.0 ± 0.2	1276.0 ± 0.3

Means and standard deviations from four independent experiments conducted in triplicate.
[a] AEVD-AFC emits blue light (λmax = 400 nm); upon cleavage of the substrate by caspase-10, free AFC emits a yellow-green fluorescence (λmax = 505 nm).

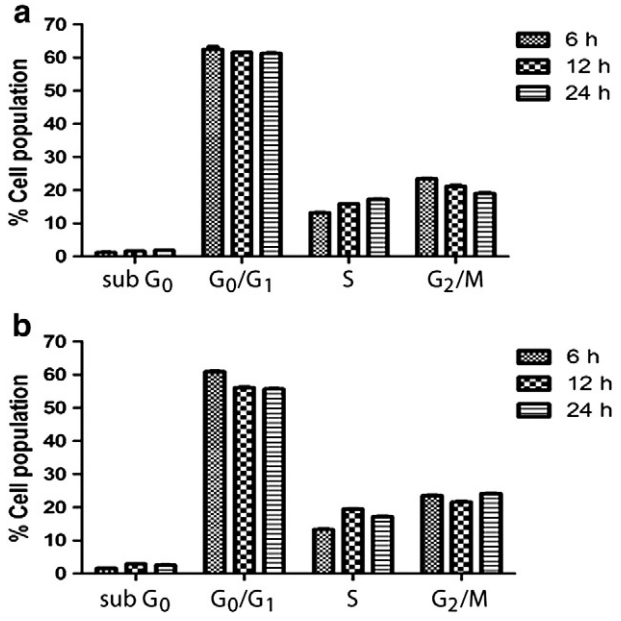

Fig. 11. Effect of (a) 1 and (b) 2 on cell cycle distribution in HepG2 cells. Cells were incubated at doses corresponding to the IC_{50} value (0.53 and 55.9 μM, respectively) for 6, 12 and 24 h, and the distribution of the cell cycle was ascertained by FACS analysis. The data are representative examples for triplicate independent tests. *$p < 0.05$ versus control group.

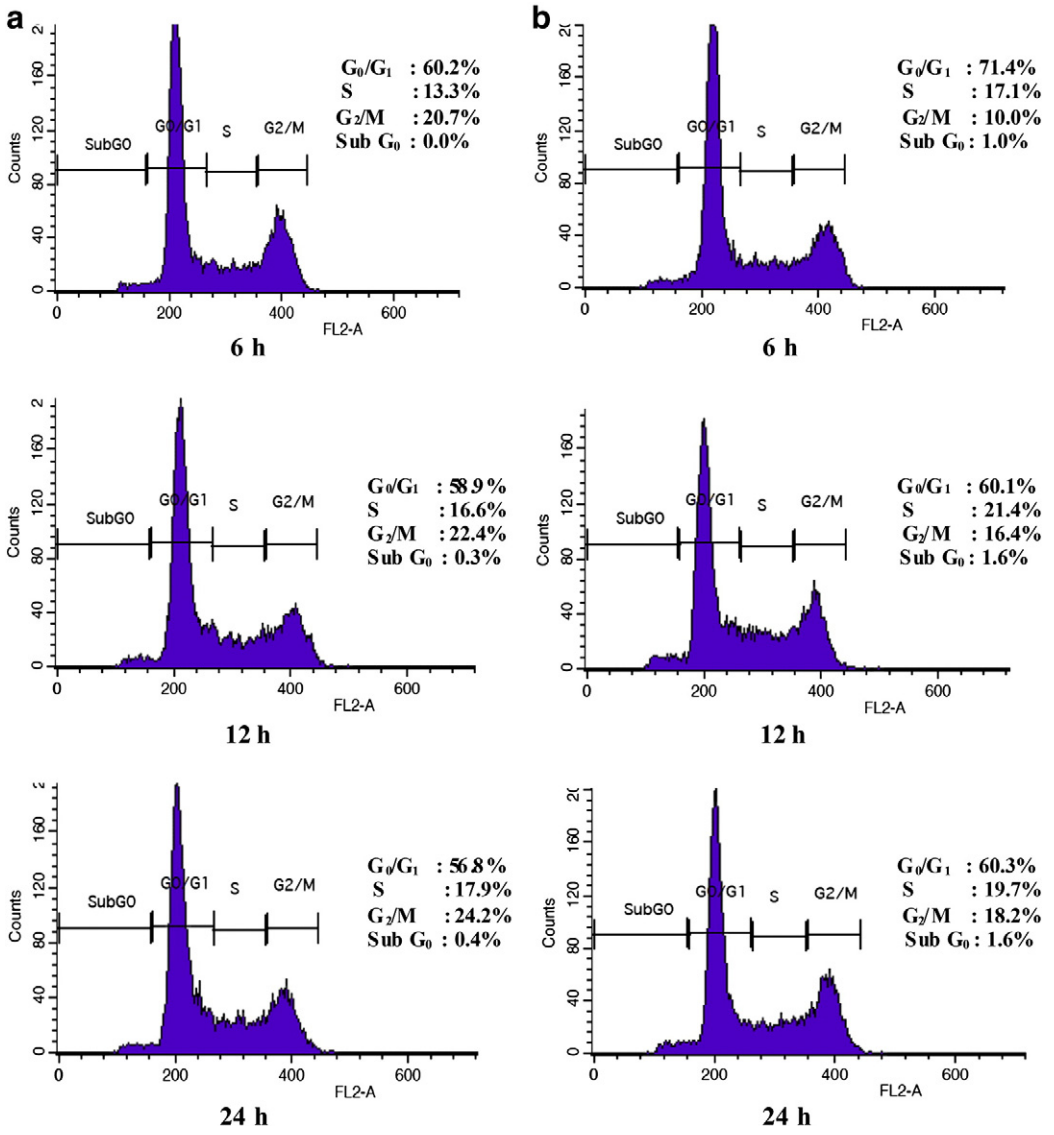

Fig. 12. Effect of 1 and 2 on cell cycle distribution in cultured HepG2 cells. Cells were incubated at doses corresponding to the IC_{50} value (0.53 and 55.9 μM, respectively) for 6, 12 and 24 h, and the distribution of the cell cycle were ascertained by FACS analysis.

In addition to this intrinsic pathway, both 1 and 2 stimulated death receptor p53 resulting in the activation of an extrinsic pathway. Initially, p53/p73 is activated in response to the presence of 1 and 2. In turn, p53 promotes expression of Bax, which leads to an imbalance of Bax/Bcl-2 and possible mitochondrial dysfunction. Finally, after activation of caspase-3, lead-induced apoptosis occurs. Complementing this pathway, p53 also stimulates the expression of Fas followed by the activation of receptor-bound FADD and TRADD. FADD is responsible for recruiting procaspases-8 and -10 and leads to their auto-cleavage and activation, and subsequently activates effector caspases in initiating cell death.

Apart from the mitochondrial and FAS death receptor apoptotic pathways, 1 was also found to induce another death receptor-dependent pathway by induction of CD40, CD40L and TNF-R1 (p55). In addition, DAPK1, a tumour suppressor, was highly expressed by 1 in HepG2 cells together with down-regulation of XIAP and NF-κB; inactivation of XIAP in cancer cells results in apoptosis. By contrast, XIAP was significantly expressed by 2 under the same experimental conditions. Over-expression of siDAPk1 significantly rescued the protein expression of transcription factor NF-κB-targeted genes.

The inhibition in the growth of HepG2 cancer cells mediated by 1 and 2 occurred via cell cycle arrest at the S and G_2/M phases with the accumulation of cells in these phases being matched by a concomitant decreases in the percentage of cells in the G_0/G_1 phase according time-dependent experiments conducted up to 24 h. These findings are supported by the cell cycle RT^2 profiler PCR microarray focused on cyclin-dependent kinase-related pathway genes, PI-3 PIKK family, serine/threonine-protein kinase and mini-chromosome maintenance (MCM) proteins.

An invasion assay was also performed with the findings showing that the cell invasion rate of 2 is 10-fold higher than 1. The down-regulation of survivin and XIAP expression by 1 leads to the inhibition of metastasis in HepG2 cells.

The present study showed that 1 and 2 interact with DNA through different binding motifs. Thus, the reactivity of the Ssp I, Nde I and Bst 11071 (AT or TA specific) restriction enzymes was mitigated after treatment with 1, thereby indicating that the AT or TA specific sites were occupied by 1 followed by the inhibition of restriction enzyme digestion. On the other hand, 2 did not interfere with any restriction enzyme demonstrating that they are neither AT- nor GC-specific and therefore, the compound might not interact with or just randomly bind to DNA. This finding provides a further explanation as to why 1 is a better cytotoxic agent than 2 in HepG2 cells.

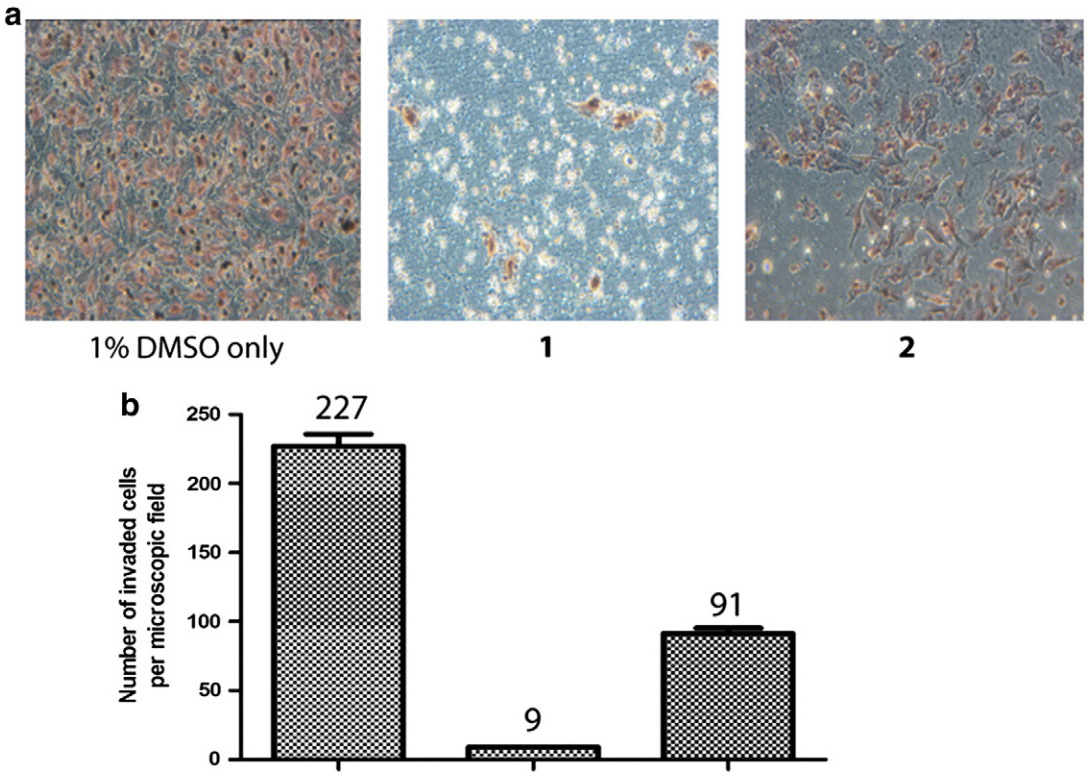

Fig. 13. Matrigel invasion assay showing that 1 and 2 inhibited cell invasion. (a) Photos were taken at 200× magnification, and are representative of three independent experiments. (b) Graphical representation of the numbers of invaded cells per microscopic fields when treated with 1 and 2. Data were shown as mean ± SEM from three independent experiments. $^{*}p < 0.05$, compared to the DMSO only. The invasion rates of 1 and 2 are 3.96 ± 0.52 and 40.22 ± 2.36%, respectively (normalized to 100%).

5. Conclusions

$Bi(S_2CNEt_2)_3$ (1) is shown to be cytotoxic against a range of human carcinoma but, $Bi(S_2CNCH_2CH2OH)_3$ (2) is considerably less cytotoxic. Against HepG2, mechanisms of cell death induced by 1 and 2 occur by mitochondrial and FAS apoptotic pathways. In addition, 1 highly expressed the tumour suppressor DAPK1, down-regulated both XIAP and NF-κB, and also induced CD40, CD40L and TNF-R1 (p55). Growth inhibition of HepG2 is correlated with cell cycle arrest at the S and G_2/M phases. The cell invasion rate of 1 is 10-fold less than 2, and 1 interacts with DNA at AT- or TA-specific sites.

Abbreviations

AIF	Apoptosis-inducing factor
APAF-1	Apoptosis activating factor-1
ATM	gene ataxia telangiectasia mutated gene
ATR	protein Rad-3 related protein
Bax	Bcl-2 associated X protein
Bcl-2	b-cell lymphoma 2
BID	BH3 interacting domain death agonist
BNIP3L	protein BCL2/adenovirus E1B 19 kDa interacting protein 3-like
BRIC5	benign recurrent intrahepatic cholestasis protein 5
c-Abl protein	c-abl oncogene 1, non-receptor tyrosine kinase
Carboxy-H_2DCFDA	5-(and-6)-carboxy-2′,7′-dichlorodihydrofluorescein diacetate
$CCNB_1$	cyclin B_1
$CCND_1$	cyclin D_1
$CCNE_1$	cyclin E_1
CD40	tumour necrosis factor receptor superfamily, member 5
CD40L	tumour necrosis factor superfamily, member 5
Cdc2	cell division control protein 2 homolog
CDKN1A	cyclin-dependent kinase inhibitor 1A
CDKN1A	cyclin-dependent kinase inhibitor p21
Chek1	serine/threonine protein kinase
COX-2	cyclooxygenase-2
c-Src	c-Src tyrosine kinase
DAPK1	death-associated protein kinase 1
DFFA	DNA fragmentation factor subunit alpha
EtBr	ethidium bromide
FADD	Fas-associated protein with death domain
FAK	Focal adhesion kinase
FAS	tumour necrosis factor superfamily, member 6
GADD45	growth arrest and DNA Damage protein 45
ICAM-1	intercellular adhesion molecule-2
MCM	protein Mini-chromosome maintenance
MMT	3-[4,5-dimethylthiazole-2-yl]-2,5-diphenyltetrazolium bromide
PCR	polymerase chain reaction
PIKK	PI-3 protein kinase-like kinase
ROS	reactive oxygen species
TAE	Tris-acetate EDTA
tBID	truncated BH3 interacting-domain death agonist
TNF-R1	tumour necrosis factor receptor superfamily, member 1A
TNFRSF1A	tumour necrosis factor receptor
XIAP	X-lined mammalian inhibitor of apoptosis protein

Supplementary data to this article can be found online at http://dx.doi.org/10.1016/j.jinorgbio.2013.09.018.

Conflict of interest

The authors have no conflict of interest to disclose.

Acknowledgements

The authors thank the Ministry of Higher Education of Malaysia and the University of Malaya (UM.C/HIR-MOHE/SC/03) for funding these studies.

References

[1] A. Slikkerveer, F.A. de Wolff, Med. Toxicol. Adverse Drug Exp. 4 (1989) 303–323.
[2] H. Menge, B. Brosius, A. Lang, M. Gregor, Gastroenterology 102 (1992) 2192–2193.
[3] H. Sun, L. Zhang, K.Y. Szeto, Met. Ions Biol. Syst. 41 (2004) 333–378.
[4] W.A. Herrmann, E. Herdtweck, L. Pajdla, Inorg. Chem. 30 (1991) 2579–2581.
[5] A.G. Degraaff, F.B. Hulsbergen, J. Reedijk, Inorg. Chem. 30 (1991) 4210–4218.
[6] E. Asato, K. Katsura, M. Mikuriya, T. Fujii, J. Reedijk, Inorg. Chem. 32 (1993) 5322–5329.
[7] E.R.T. Tiekink, Crit. Rev. Oncol. Hematol. 42 (2002) 217–224.
[8] N. Yang, J.A. Tanner, B.J. Zheng, R.M. Watt, M.L. He, L.Y. Lu, J.Q. Jiang, K.T. Shum, Y.P. Lin, K.L. Wong, M.C. Lin, H.F. Kung, H. Sun, J.D. Huang, Angew. Chem. Int. Ed. Engl. 46 (2007) 6464–6468.
[9] P.C. Andrews, M. Busse, G.B. Deacon, R.L. Ferrero, P.C. Junk, J.G. MacLellan, A. Vom, Dalton Trans. 41 (2012) 11798–11806.
[10] P.C. Andrews, R. Frank, P.C. Junk, L. Kedzierski, I. Kumar, J.G. MacLellan, J. Inorg. Biochem. 105 (2011) 454–461.
[11] T. Murafuji, Y. Fujiwara, D. Yoshimatsu, I. Miyakawa, K. Migita, Y. Mikata, Eur. J. Med. 46 (2011) 519–525.
[12] In: H. Sun (Ed.), Biological Chemistry of Arsenic, Antimony and Bismuth, John Wiley & Sons, New York, 2011.
[13] H. Li, H. Sun, Curr. Opin. Chem. Biol. 16 (2012) 74–83.
[14] H. Li, P.J. Sadler, H. Sun, J. Biol. Chem. 271 (1996) 9483–9489.
[15] H. Sun, H. Li, A.B. Mason, R.C. Woodworth, P.J. Sadler, Biochem. J. 337 (1999) 105–111.
[16] E. Cedergren-Zeppezauer, J.P. Samama, H. Eklund, Biochemistry 21 (1982) 4895–4908.
[17] P.J. Saddler, H. Sun, H. Li, Chem. Eur. J. 2 (1996) 701.
[18] A. Gyurasics, L. Koszorus, F. Varga, Z. Gregus, Biochem. Pharmacol. 44 (1992) 1275–1281.
[19] H. Sun, N. Yang, Coord. Chem. Rev. 251 (2007) 2354–2366.
[20] E.R.T. Tiekink, in: H. Sun (Ed.), Anticancer activity of molecular compounds of arsenic, antimony and bismuth, Biological Chemistry of Arsenic, Antimony and BismuthJohn Wiley & Sons, New York, 2011, pp. 293–310.
[21] W. Friebolin, G. Schilling, M. Zoller, E. Amtmann, J. Med. Chem. 48 (2005) 7925–7931.
[22] H. Li, C.S. Lai, J. Wu, P.C. Ho, D. de Vos, E.R.T. Tiekink, J. Inorg. Biochem. 101 (2007) 809–816.
[23] X'Pert HighScore Plus, PANalytical B.V., Almelo, The Netherlands, 2009.
[24] C.L. Raston, A.H. White, J. Chem. Soc. Dalton Trans. (1976) 791–794.
[25] V. Venkatachalam, K. Ramalingam, U. Casellato, R. Graziani, Polyhedron 16 (1997) 1211–1221.
[26] J. Kapuscinski, Z. Darzynkiewicz, M.R. Melamed, F. Traganos, Biochem. Pharmacol. 32 (1983) 3679–3694.
[27] C.J. Yeh, B.L. Hsi, W.P. Faulk, J. Immunol. Methods 43 (1981) 269–275.
[28] C. Foglieni, C. Meoni, A.M. Davalli, Histochem. Cell Biol. 115 (2001) 223–229.
[29] K. Samejima, W.C. Earnshaw, Nat. Rev. Mol. Cell Biol. 6 (2005) 677–688.
[30] E.K. Rowinsky, J. Clin. Oncol. 23 (2005) 9394–9407.
[31] K. Palanichamy, N. Sreejayan, A.C. Ontko, J. Inorg. Biochem. 106 (2012) 32–42.
[32] S.W. Fesik, Nat. Rev. Cancer 5 (2005) 876–885.
[33] L. Qiao, B.C. Wong, Drug Resist. Updat. 12 (2009) 55–64.
[34] K.K. Wong, Recent Pat. Anticancer Drug Discov. 4 (2009) 28–35.
[35] G. Kroemer, L. Galluzzi, P. Vandenabeele, J. Abrams, E.S. Alnemri, E.H. Baehrecke, M.V. Blagosklonny, W.S. El-Deiry, P. Golstein, D.R. Green, M. Hengartner, R.A. Knight, S. Kumar, S.A. Lipton, W. Malorni, G. Nunez, M.E. Peter, J. Tschopp, J. Yuan, M. Piacentini, B. Zhivotovsky, G. Melino, D. Nomenclature Committee on Cell, Cell Death Differ. 16 (2009) 3–11.
[36] A.L. Gartel, A.L. Tyner, Mol. Cancer Ther. 1 (2002) 639–649.
[37] C. Barlow, K.D. Brown, C.X. Deng, D.A. Tagle, A. Wynshaw-Boris, Nat. Genet. 17 (1997) 453–456.
[38] M. Dobbelstein, S. Strano, J. Roth, G. Blandino, Biochem. Biophys. Res. Commun. 331 (2005) 688–693.
[39] P. Fei, W. Wang, S.H. Kim, S. Wang, T.F. Burns, J.K. Sax, M. Buzzai, D.T. Dicker, W.G. McKenna, E.J. Bernhard, W.S. El-Deiry, Cancer Cell 6 (2004) 597–609.
[40] Y. Tsujimoto, S. Shimizu, FEBS Lett. 466 (2000) 6–10.
[41] R. Eskes, B. Antonsson, A. Osen-Sand, S. Montessuit, C. Richter, R. Sadoul, G. Mazzei, A. Nichols, J.C. Martinou, J. Cell Biol. 143 (1998) 217–224.
[42] A. Gross, J.M. McDonnell, S.J. Korsmeyer, Genes Dev. 13 (1999) 1899–1911.
[43] P.X. Petit, S.A. Susin, N. Zamzami, B. Mignotte, G. Kroemer, FEBS Lett. 396 (1996) 7–13.
[44] G. Kroemer, L. Galluzzi, C. Brenner, Physiol. Rev. 87 (2007) 99–163.
[45] L.Y. Li, X. Luo, X. Wang, Nature 412 (2001) 95–99.
[46] G. van Loo, P. Schotte, M. van Gurp, H. Demol, B. Hoorelbeke, K. Gevaert, I. Rodriguez, A. Ruiz-Carrillo, J. Vandekerckhove, W. Declercq, R. Beyaert, P. Vandenabeele, Cell Death Differ. 8 (2001) 1136–1142.
[47] X. Saelens, N. Festjens, L. Vande Walle, M. van Gurp, G. van Loo, P. Vandenabeele, Oncogene 23 (2004) 2861–2874.
[48] V.P. Skulachev, FEBS Lett. 397 (1996) 7–10.
[49] M. Le Bras, M.V. Clement, S. Pervaiz, C. Brenner, Histol. Histopathol. 20 (2005) 205–219.
[50] P.H. Krammer, Adv. Immunol. 71 (1999) 163–210.
[51] F. Caruso, R. Villa, M. Rossi, C. Pettinari, F. Paduano, M. Pennati, M.G. Daidone, N. Zaffaroni, Biochem. Pharmacol. 73 (2007) 773–781.
[52] A. Thorburn, Cell. Signal. 16 (2004) 139–144.
[53] R.M. Abd El-Ghany, N.M. Sharaf, L.A. Kassem, L.G. Mahran, O.A. Heikal, Drug Discov. Ther. 3 (2009) 296–306.
[54] X.M. Yin, Gene 369 (2006) 7–19.
[55] C.P. LeBel, H. Ischiropoulos, S.C. Bondy, Chem. Res. Toxicol. 5 (1992) 227–231.
[56] A. Gomes, E. Fernandes, J.L. Lima, J. Biochem. Biophys. Methods 65 (2005) 45–80.
[57] A.S. Loskog, A.G. Eliopoulos, Semin. Immunol. 21 (2009) 301–307.
[58] I. Airoldi, S. Lualdi, S. Bruno, L. Raffaghello, M. Occhino, C. Gambini, V. Pistoia, M.V. Corrias, Br. J. Cancer 88 (2003) 1527–1536.
[59] A.G. Eliopoulos, C.W. Dawson, G. Mosialos, J.E. Floettmann, M. Rowe, R.J. Armitage, J. Dawson, J.M. Zapata, D.J. Kerr, M.J. Wakelam, J.C. Reed, E. Kieff, L.S. Young, Oncogene 13 (1996) 2243–2254.
[60] S. Hess, E. Gottfried, H. Smola, U. Grunwald, M. Schuchmann, H. Engelmann, Eur. J. Immunol. 28 (1998) 3594–3604.
[61] M. Grell, G. Zimmermann, E. Gottfried, C.M. Chen, U. Grunwald, D.C. Huang, Y.H.Wu. Lee, H. Durkop, H. Engelmann, P. Scheurich, H. Wajant, A. Strasser, EMBO J. 18 (1999) 3034–3043.
[62] S. Hess, H. Engelmann, J. Exp. Med. 183 (1996) 159–167.
[63] H.J. Yoo, H.J. Byun, B.R. Kim, K.H. Lee, S.Y. Park, S.B. Rho, Cell. Signal. 24 (2012) 1471–1477.
[64] N. Kodama, A. Asakawa, A. Inui, Y. Masuda, H. Nanba, Oncol. Rep. 13 (2005) 497–502.
[65] E.C. LaCasse, S. Baird, R.G. Korneluk, A.E. MacKenzie, Oncogene 17 (1998) 3247–3259.
[66] B.P. Eckelman, G.S. Salvesen, F.L. Scott, EMBO Rep. 7 (2006) 988–994.
[67] L. Yang, Z. Cao, H. Yan, W.C. Wood, Cancer Res. 63 (2003) 6815–6824.
[68] E.C. LaCasse, Cancer Lett. 332 (2013) 215–224.
[69] L.R. Gouvea, L.S. Garcia, D.R. Lachter, P.R. Nunes, F. de Castro Pereira, E.P. Silveira-Lacerda, S.R. Louro, P.J. Barbeira, L.R. Teixeira, Eur. J. Med. Chem. 55 (2012) 67–73.
[70] V. Gandin, A.P. Fernandes, M.P. Rigobello, B. Dani, F. Sorrentino, F. Tisato, M. Bjornstedt, A. Bindoli, A. Sturaro, R. Rella, C. Marzano, Biochem. Pharmacol. 79 (2010) 90–101.
[71] E. Bremer, G. van Dam, B.J. Kroesen, L. de Leij, W. Helfrich, Trends Mol. Med. 12 (2006) 382–393.
[72] A. Sakaue-Sawano, T. Kobayashi, K. Ohtawa, A. Miyawaki, BMC Cell Biol. 12 (2011) 2.
[73] H.L. Oh, D.K. Lee, H. Lim, C.H. Lee, J. Ethnopharmacol. 129 (2010) 135–139.
[74] C.C. Cheng, S.M. Yang, C.Y. Huang, J.C. Chen, W.M. Chang, S.L. Hsu, Cancer Chemother. Pharmacol. 55 (2005) 531–540.
[75] X. Grana, E.P. Reddy, Oncogene 11 (1995) 211–219.
[76] P. Jin, Y. Gu, D.O. Morgan, J. Cell Biol. 134 (1996) 963–970.
[77] J.H. Cho, J.G. Lee, Y.I. Yang, J.H. Kim, J.H. Ahn, N.I. Baek, K.T. Lee, J.H. Choi, Food Chem. Toxicol. 49 (2011) 1737–1744.
[78] B.C. Dash, W.S. El-Deiry, Mol. Cell. Biol. 25 (2005) 3364–3387.
[79] A.B. Niculescu, X. Chen, M. Smeets, L. Hengst, C. Prives, S.I. Reed, Mol. Cell. Biol. 18 (1998) 629–643.
[80] R. Zhao, N. Xiang, F.E. Domann, W. Zhong, Nutr. Cancer 61 (2009) 397–407.
[81] N.S. Ting, W.H. Lee, DNA Repair (Amst) 3 (2004) 935–944.
[82] R.I. Yarden, S. Pardo-Reoyo, M. Sgagias, K.H. Cowan, L.C. Brody, Nat. Genet. 30 (2002) 285–289.
[83] C.S. Sorensen, R.G. Syljuasen, Nucleic Acids Res. 40 (2012) 477–486.
[84] V. Padmanabhan, P. Callas, G. Philips, T.D. Trainer, B.G. Beatty, J. Clin. Pathol. 57 (2004) 1057–1062.
[85] H. Takisawa, S. Mimura, Y. Kubota, Curr. Opin. Cell Biol. 12 (2000) 690–696.
[86] T.M. Passalaris, J.A. Benanti, L. Gewin, T. Kiyono, D.A. Galloway, Mol. Cell. Biol. 19 (1999) 5872–5881.
[87] Q. Zhan, I. Bae, M.B. Kastan, A.J. Fornace Jr., Cancer Res. 54 (1994) 2755–2760.
[88] Q. Zhan, S. Fan, M.L. Smith, I. Bae, K. Yu, I. Alamo Jr., P.M. O'Connor, A.J. Fornace Jr., DNA Cell Biol. 15 (1996) 805–815.
[89] Q. Zhan, M.J. Antinore, X.W. Wang, F. Carrier, M.L. Smith, C.C. Harris, A.J. Fornace Jr., Oncogene 18 (1999) 2892–2900.
[90] B.L. Eckhardt, P.A. Francis, B.S. Parker, R.L. Anderson, Nat. Rev. Drug Discov. 11 (2012) 479–497.
[91] S. Mehrotra, L.R. Languino, C.M. Raskett, A.M. Mercurio, T. Dohi, D.C. Altieri, Cancer Cell 17 (2010) 53–64.
[92] W. Tan, W. Zhang, A. Strasner, S. Grivennikov, J.Q. Cheng, R.M. Hoffman, M. Karin, Nature 470 (2011) 548–553.
[93] E. Meylan, A.L. Dooley, D.M. Feldser, L. Shen, E. Turk, C. Ouyang, T. Jacks, Nature 462 (2009) 104–107.
[94] E. Pikarsky, R.M. Porat, I. Stein, R. Abramovitch, S. Amit, S. Kasem, E. Gutkovich-Pyest, S. Urieli-Shoval, E. Galun, Y. Ben-Neriah, Nature 431 (2004) 461–466.
[95] Y. Wu, J. Deng, P.G. Rychahou, S. Qiu, B.M. Evers, B.P. Zhou, Cancer Cell 15 (2009) 416–428.
[96] B.K. Park, H. Zhang, Q. Zeng, J. Dai, E.T. Keller, T. Giordano, K. Gu, V. Shah, L. Pei, R.J. Zarbo, L. McCauley, S. Shi, S. Chen, C.Y. Wang, Nat. Med. 13 (2007) 62–69.